Available online at www.sciencedirect.com
ScienceDirect
Polymer 48 (2007) 1620–1631
polymer
www.elsevier.com/locate/polymer

Theoretical phase diagram calculation and membrane morphology evaluation for water/solvent/polyethersulfone systems

J. Barzin*, B. Sadatnia

Department of Biomaterials, Iran Polymer and Petrochemical Institute, P.O. Box 14965/115, Tehran, Iran

Received 16 December 2006; received in revised form 22 January 2007; accepted 25 January 2007
Available online 30 January 2007

Abstract

Theoretical ternary phase diagrams with very good agreement with experimental cloud point data were constructed for water/*N*,*N*-dimethylacetamide (DMAc)/polyethersulfone (PES) and water/*N*-methyl-2-pyrrolidone (NMP)/polyethersulfone systems. Theoretical phase diagrams were determined based on the extended Flory–Huggins theory of polymer solutions. To construct the theoretical phase diagrams, all binary interaction parameters were determined accurately and thoroughly revisited. Also, the structures of membranes prepared of these systems by phase separation process were investigated. The morphological studies showed that in spite of better miscibility between water and DMAc compared to water and NMP, channel-like structures were observed in membranes prepared of water/NMP/PES systems but tear-like structures with more spongy areas were observed in membranes prepared of water/DMAc/PES system. According to the constructed theoretical ternary phase diagrams of these systems, these unexpected observations were attributed to the higher concentration of polymer in the polymer-rich phase of water/DMAc/PES system, which causes an early vitrification in this system which suppresses the growth of macrovoids.

Keywords: Ternary phase diagram; Interaction parameter; Membrane structure

1. Introduction

Phase separation process, which sometimes called the phase inversion process, is without doubt the most important technique for the preparation of both asymmetric (anisotropic) and symmetric (isotropic) polymeric membranes [1]. In this method a flat-sheet or hollow fiber membrane is constructed by precipitation of a homogeneous polymer solution into a solid, polymer-rich phase and a liquid, polymer-lean phase [2]. Although there are several methods for the precipitation of a polymer solution, casting the desired polymer solution on a suitable support and immersing it in a nonsolvent bath is the usual method for the preparation of polymeric membranes in the phase separation process.

It is widely accepted that the kinetics and thermodynamics of the phase separation process have major roles in determining the final structure of the membrane prepared by this process and several researchers [3–11] have studied various kinetic and thermodynamic aspects of this process for a wide variety of ternary systems. Membrane morphology, on the other hand, has a large effect on the membrane performance, and therefore a complete knowledge concerning the kinetics and thermodynamics of the desired membrane-forming system is required.

For thermodynamic evaluations of a membrane-forming system, the Flory–Huggins theory of polymer solutions [12], which has been extended to a ternary system containing nonsolvent/solvent/polymer by Tompa [13], is usually used and a ternary phase diagram including binodal and spinodal curves and tie lines is constructed. Binary interaction parameters of nonsolvent/solvent, solvent/polymer, and nonsolvent/polymer are the main input parameters of the Flory–Huggins relation. The magnitude and concentration dependency of these interaction parameters have a large effect on the binodal, spinodal, and critical point positions of a phase diagram.

* Corresponding author. Tel.: +98 21 44580050; fax: +98 21 44580161.
E-mail address: j.barzin@ippi.ac.ir (J. Barzin).

0032-3861/$ - see front matter © 2007 Elsevier Ltd. All rights reserved.
doi:10.1016/j.polymer.2007.01.049

The effects of these parameters on the phase diagram of a membrane-forming system have been studied by several researchers [6–11] for various ternary systems. Altena and Smolders [6] were the first who performed a comprehensive thermodynamic study for a wide range of ternary membrane-forming systems. They have studied water/solvent/cellulose acetate and water/solvent/polysulfone systems and their theoretical calculations showed that good agreement can be found between experimental and theoretical miscibility gaps when the nonsolvent/solvent interaction parameter is taken concentration dependent and two other interaction parameters are considered concentration independent. On the other hand, Yilmaz and McHugh [8] have shown that the concentration dependency of the solvent/polymer interaction parameter is more important than that of the nonsolvent/solvent parameter. Other researchers [9–11] have performed similar studies for other ternary systems and revealed some other thermodynamic aspects of ternary membrane-forming systems.

In our group we have mainly focused on the fabrication of flat-sheet and hollow fiber membranes for hemodialysis by nonsolvent-induced phase separation process based on polyethersulfone (PES) as the main polymer. PES has many fascinating properties including favorable mechanical strength, thermal and chemical resistance, and excellent biocompatibility [14,15] and in recent years PES has been used in a wide rang of membrane applications such as gas separation, purification of various liquids, separation of biological components, medical devices and hemodialysis [16–19]. In our previous works, we have studied the preparation of flat-sheet and hollow fiber hemodialysis membranes with PES and evaluated the effect of additives and preparation conditions on the membranes morphology and performance and their results are reported elsewhere [20–22].

Although nonsolvent/solvent/PES systems are widely used in industrial membrane applications, there are a few thermodynamic studies concerning these industrially important systems in the literature [9,23]. For this reason, in the present study, a comprehensive thermodynamic analysis of systems containing water/DMAc/PES and water/NMP/PES has been performed. Binary interaction parameters of these systems have been measured experimentally. The ternary phase diagrams were then constructed theoretically and compared with the experimental results and meanwhile some controversies exist in the literature on the magnitude of interaction parameters of these systems have been clarified. On the other hand, according to the constructed theoretical phase diagrams, some unexpected structures observed for membranes prepared of these systems have been verified as well.

2. Theory

2.1. Thermodynamics of nonsolvent/solvent/polymer systems

An extended form of Flory–Huggins theory of polymer solutions [12,13] is typically used to predict the thermodynamic behavior of nonsolvent/solvent/polymer systems. According to this theory, the Gibbs free energy of mixing, ΔG_m, for a ternary system is given by the following relation:

$$\frac{\Delta G_m}{RT} = n_1 \ln \phi_1 + n_2 \ln \phi_2 + n_3 \ln \phi_3 + g_{12} n_1 \phi_2 + g_{13} n_1 \phi_3 + g_{23} n_2 \phi_3 \quad (1)$$

where n_i and ϕ_i are the number of moles and volume fraction of component i, respectively. R is the gas constant and T is the absolute temperature. g_{ij} are concentration-dependent binary interaction parameters between components i and j. The subscripts refer to nonsolvent (1), solvent (2), and polymer (3).

The nonsolvent/solvent interaction parameter, g_{12}, is usually assumed to be a function of u_2, where u_2 is the volume fraction of solvent on a polymer-free basis ($u_2 = \phi_2/(\phi_1 + \phi_2)$) [6,8,24]. The nonsolvent/polymer interaction parameter, g_{13}, although by definition must be a concentration-dependent parameter, but in most thermodynamic evaluations of ternary systems, no concentration dependency was considered for this parameter. In some studies, solvent/polymer interaction parameter, g_{23}, has been considered as a function of ϕ_3, the ternary polymer volume fraction [8,24] and in some other studies, this parameter has been expressed as a function of v_3, the volume fraction of polymer on a nonsolvent-free basis [11,25,26]. In the present work, concentration dependency has been considered for g_{12}, but g_{23} and g_{13} assumed to be concentration-independent interaction parameters. Therefore, in the following equations, χ_{23} and χ_{13} are used instead of g_{23} and g_{13}.

2.1.1. Binodal curve

When some component i is distributed between two phases, the thermodynamic equation of equilibrium is expressed as follows [27]:

$$\Delta\mu_{i,A} = \Delta\mu_{i,B} \quad i = 1, 2, 3 \quad (2)$$

where $\Delta\mu_i$ is the difference between the chemical potential of component i in the mixture and the pure state. The subscripts A and B refer to the polymer-rich and polymer-lean phases, respectively.

By definition, the derivative of the Gibbs free energy of mixing with respect to the number of moles of each component results in the chemical potential of component i [27]:

$$\frac{\Delta\mu_i}{RT} = \frac{\partial}{\partial n_i}\left(\frac{\Delta G_m}{RT}\right)_{P,T,n_j} \quad (3)$$

From Eqs. (1) and (3), the chemical potential of components in the mixture can be derived as follows [6,8,10,11]:

$$\frac{\Delta\mu_1}{RT} = \ln\phi_1 + 1 - \phi_1 - \frac{v_1}{v_2}\phi_2 - \frac{v_1}{v_3}\phi_3 + (g_{12}\phi_2 + \chi_{13}\phi_3) \times (\phi_2 + \phi_3) - \chi_{23}\frac{v_1}{v_2}\phi_2\phi_3 - u_1 u_2 \phi_2 \left(\frac{dg_{12}}{du_2}\right) \quad (4)$$

$$\frac{\Delta\mu_2}{RT} = \ln\phi_2 + 1 - \phi_2 - \frac{v_2}{v_1}\phi_1 - \frac{v_2}{v_3}\phi_3 + \left(g_{12}\frac{v_2}{v_1}\phi_1 + g_{23}\phi_3\right) \times (\phi_1 + \phi_3) - \chi_{13}\frac{v_2}{v_1}\phi_1\phi_3 + u_1u_2\phi_1\frac{v_2}{v_1}\left(\frac{dg_{12}}{du_2}\right) \quad (5)$$

$$\frac{\Delta\mu_3}{RT} = \ln\phi_3 + 1 - \phi_3 - \frac{v_3}{v_1}\phi_1 - \frac{v_3}{v_2}\phi_2 + \left(\chi_{13}\frac{v_3}{v_1}\phi_1 + \chi_{23}\frac{v_3}{v_2}\phi_2\right) \times (\phi_1 + \phi_2) - g_{12}\frac{v_3}{v_1}\phi_1\phi_2 \quad (6)$$

where v_i is the molar volume of component i. It should be noted that only binary interaction parameters are considered in these equations.

2.1.2. Method of calculation of binodal curve

Every composition inside the binodal will demix into a polymer-rich and a polymer-lean phase, which are in thermodynamic equilibrium with each other [7]. The line which connects a pair of equilibrium compositions in the polymer-rich phase ($\phi_{1,A}$, $\phi_{2,A}$, $\phi_{3,A}$) and polymer-lean phase ($\phi_{1,B}$, $\phi_{2,B}$, $\phi_{3,B}$) is a tie line.

To specify the tie line compositions, these six unknowns should be determined. There are five relations between these six unknown compositions. Three of them are given by substituting Eqs. (4)–(6) in Eq. (2). Two remaining equations are the material balance relations in the polymer-rich and polymer-lean phases.

$$\Sigma\phi_{i,A} = \Sigma\phi_{i,B} = 1 \quad i = 1, 2, 3 \quad (7)$$

To find these six unknown compositions, the polymer composition in the polymer-lean phase, $\phi_{3,B}$, was considered as an independent variable [6,8] and the remaining system of five equations were solved by the Newton–Raphson method.

2.1.3. Spinodal curve

The boundary between unstable and metastable regions is the so-called spinodal, which is thermodynamically defined as

$$\frac{\partial^2\Delta G}{\partial\phi^2} = 0 \quad (8)$$

Spinodal curve can be obtained from the following relation [13,28]:

$$G_{22}G_{33} = (G_{23})^2 \quad (9)$$

where $G_{ij} = (\partial^2\overline{\Delta G}_m/\partial\phi_i\partial\phi_j)_{v_{ref}}$ and $\overline{\Delta G}_m$ is the Gibbs free energy of mixing on a unit volume basis and v_{ref} is the molar volume of the reference component which is be taken to be component 1. Therefore, from the relationship for $\overline{\Delta G}_m$, the following expressions result [8].

$$G_{22} = \frac{1}{\phi_1} + \frac{v_1}{v_2\phi_2} - 2g_{12} + 2(u_1 - u_2)\left(\frac{dg_{12}}{du_2}\right) + u_1u_2\left(\frac{d^2g_{12}}{du_2^2}\right) \quad (10)$$

$$G_{23} = \frac{1}{\phi_1} - (g_{12} + \chi_{13}) + \frac{v_1}{v_2}\chi_{23} + u_2(u_1 - 2u_2)\left(\frac{dg_{12}}{du_2}\right) + u_1u_2^2\left(\frac{d^2g_{12}}{du_2^2}\right) \quad (11)$$

$$G_{33} = \frac{1}{\phi_1} + \frac{v_1}{v_3\phi_3} - 2\chi_{13} - 2u_2^2(1 - u_1)\left(\frac{dg_{12}}{du_2}\right) + u_1u_2^3\left(\frac{d^2g_{12}}{du_2^2}\right) \quad (12)$$

Substitution of Eqs. (10) to (12) in Eq. (9) along with material balance equation results in two equations with three variables which can be solved numerically (again with Newton–Raphson method) by choosing one of the variables (in our case ϕ_3) as the independent variable.

2.1.4. Critical point

The critical point where the binodal and spinodal curves touch each other thermodynamically is expressed as

$$\frac{\partial^2\Delta G}{\partial\phi^2} = \frac{\partial^3\Delta G}{\partial\phi^3} = 0 \quad (13)$$

The critical point composition can be calculated using the following equation [8]:

$$G_{222}G_{33}^2 - 3G_{223}G_{23}G_{33} + 3G_{233}G_{23}^2 - G_{22}G_{23}G_{333} = 0 \quad (14)$$

2.2. Binary interaction parameters

2.2.1. Nonsolvent/solvent interaction parameter

The concentration-dependent nonsolvent/solvent interaction parameter, g_{12}, is usually determined from excess Gibbs free energy (G^E) data using the following equation [1]:

$$g_{12} = \frac{1}{x_1\phi_2}\left[x_1\ln\frac{x_1}{\phi_1} + x_2\ln\frac{x_2}{\phi_2} + \frac{G^E}{RT}\right] \quad (15)$$

where x_i and ϕ_i are mole fraction and volume fraction of the components, respectively. G^E can be determined from activity coefficients data or it can be directly obtained from experimental data, which are available in the literature.

2.2.2. Solvent/polymer interaction parameter

The solvent/polymer interaction parameter, χ_{23}, may be obtained experimentally by measuring the activity of the solvent. The activity of the solvent may be determined by a number of techniques. Details of these techniques can be found in several papers, which are available in the literature [29–32].

In this study, χ_{23} has been predicted by a model proposed by Rudin et al. [33–36]. This model represents a method for predicting the osmotic pressure and osmotic and light scattering second virial coefficients of a polymer solution. The second virial coefficient, A_2, is of course related to χ_{23} by a simple equation [37]. According to this method, the osmotic pressure of a polymer solution is given by

$$\frac{\pi}{c}=\frac{RT}{\overline{M}_n}\left[1+\frac{A_2^*\overline{M}_n c}{2}\right]^2 \tag{16}$$

in which π is the osmotic pressure of a solution of polymer with number-average molecular weight $\overline{M}_n$ and concentration c, and R and T have their usual meaning [33–35]. In Eq. (16), A_2^* is given by [36]:

$$A_2^*=\frac{16\pi N_A[\eta]}{9.3\times 10^{24}M\left\{1+\frac{[\eta]-[\eta]_\theta}{[\eta]_\theta}\left[1-\exp\left(-\frac{c}{c^*}\right)\right]\right\}}\left[1-\frac{[\eta]_\theta}{[\eta]}\right] \tag{17}$$

where c is the polymer concentration (g/ml), N_A is Avogadro's number, $[\eta]$ is intrinsic viscosity of the polymer in the given solvent (ml/g), $[\eta]_\theta$ is its intrinsic viscosity under theta conditions, and M is average polymer molecular weight. c^* is a critical concentration at which the polymer coils begin to overlap each other [36].

A_2^*, as defined in this model, is a concentration-dependent parameter and therefore differs from the conventional second virial coefficient, A_2, which is independent of concentration. To obtain a concentration-independent second virial coefficient, A_2, with this method, for each concentration of the polymer solution, a value of A_2^* is calculated and then $(\pi/c)^{1/2}$ [Eq. (16)] values are plotted versus c and A_2 is determined from the slope of the straight line fitted to the results.

Solvent/polymer interaction parameter is then can be determined from the resulting second virial coefficient, A_2, by the following equation [37]:

$$\chi_{23}=\frac{1}{2}-A_2\rho_3^2V_2 \tag{18}$$

where ρ_3 is the density of polymer (g/ml) and V_2 is the molar volume of solvent (ml/mol).

The polymer molecular weight, its intrinsic viscosity in the solvent of interest, $[\eta]$, and its intrinsic viscosity under theta conditions, $[\eta]_\theta$, are the major input parameters of this model. Intrinsic viscosity of the polymer and its intrinsic viscosity under theta conditions can be calculated by the well-known Mark–Houwink–Sakurada (MHS) equation or they can be determined using viscometry measurements. Albeit in the case of $[\eta]_\theta$, the evaluations must be carried out at theta conditions. To overcome the difficulties associated with the determination of intrinsic viscosity under theta conditions, recently Qian et al. [38] have proposed a novel method for estimation of $[\eta]_\theta$ from the measurement of $[\eta]$ in a nontheta solvent. In this method $[\eta]_\theta$ is given by the following equation [38]:

$$[\eta]_\theta=\frac{[\eta]\left[1-\exp\left(-\frac{c}{c^*}\right)\right]}{\frac{0.77^3\rho}{c^*}-\exp\left(-\frac{c}{c^*}\right)} \tag{19}$$

where ρ is the coil density of a polymer molecule and is determined from the following equation:

$$\rho=\frac{c}{\eta_{sp}}\left(1.25+0.5\sqrt{56.4\eta_{sp}+6.25}\right) \tag{20}$$

where η_{sp} is specific viscosity of the polymer solution.

2.2.3. Nonsolvent/polymer interaction parameter

The nonsolvent/polymer interaction parameter, χ_{13}, is usually determined by equilibrium swelling measurement. When a nonsolvent contacts a polymer, the liquid penetrates into the polymer phase until the chemical potential of the liquid inside the polymer is equal to the chemical potential of liquid in the liquid phase [1]. This swelling behavior can be described by Flory–Rehner theory [12]. According to this theory, χ_{13} is determined with the following equation [39]:

$$\chi_{13}=-\frac{\ln(1-\phi_3)+\phi_3}{\phi_3^2} \tag{21}$$

where ϕ_3 is the volume fraction of polymer.

3. Experimental

3.1. Materials

Polyethersulfone (PES) Ultrason E 6020 P with $M_w=58{,}000$ and $M_n=16{,}111$ g/mol (BASF, Germany) was used as the polymer. *N*,*N*-Dimethylacetamide (DMAc) (Merck) and *N*-methyl-2-pyrrolidone (NMP) (Riedel-de-Haën) were used as solvents and double-distilled water was used as the nonsolvent.

3.2. Determination of cloud point curve

The cloud point curve was determined by usual titration method [7]. For this purpose, polymer solutions with concentrations of 1, 3, 5, 10, 15, 20, 25, and 30 wt% PES in DMAc and 1, 3, 5, 10, 15, 20, and 25 wt% PES in NMP were prepared by mixing desired amounts of these materials in sealed glass bottles. To achieve homogeneous polymer solutions, these mixtures were stirred for 72 h with a magnetic stirrer.

To perform the titration, double-distilled water was slowly added into the polymer solution under agitation by an adjustable volume micropipette (Calibra 822, Socorex, Switzerland) with 5 μl accuracy. During titration, the solution temperature was controlled at 25 °C with a thermostatic water bath (Julabo, Germany). The addition of pure water was continued until the clear polymer solution visually turned to a cloudy solution. After observation of the first sign of turbidity, addition of nonsolvent was stopped and the cloudy solution was agitated for an additional 30 min to see whether the turbid solution changes to a clear solution or not. If the cloudy solution turned to a clear solution, more nonsolvent was added, otherwise the determined point was considered as the onset of real cloud point. The composition of cloud point was then determined by the amount of nonsolvent, solvent, and polymer present in the bottle.

3.3. Determination of solvent/polymer interaction parameter

Solvent/polymer interaction parameters, χ_{23}, were determined by Rudin model [33–36]. In this model, first of all, A_2 is determined by the relations presented in this model, and then χ_{23} is calculated from the corresponding relation between A_2 and χ_{23} (Eq. (18)).

The major input parameters of this model are $[\eta]$, $[\eta]_\theta$, and polymer molecular weight. $[\eta]$ and $[\eta]_\theta$ were determined by viscosity measurements. Viscosities of polymer solutions with different concentrations were measured with an Ubbelohde viscometer at 25 °C. The intrinsic viscosities were then determined as the mean intercept of a dual extrapolation to zero concentration according to Huggins (Eq. (22)) and Kraemer (Eq. (23)) equations [37]:

$$\frac{\eta_{sp}}{c} = [\eta] + k_H[\eta]^2 c \tag{22}$$

$$\frac{\ln\eta_r}{c} = [\eta] + k_K[\eta]^2 c \tag{23}$$

where η_{sp} is the specific viscosity and η_r is the relative viscosity. k_H and k_K are Huggins and Kraemer constants, respectively. η_{sp} and η_r were determined from the following equations:

$$\eta_r = \frac{\eta}{\eta_0} = \frac{t}{t_0} \tag{24}$$

$$\eta_{sp} = \eta_r - 1 \tag{25}$$

where η and η_0 are the viscosity of polymer solution and of the pure solvent, respectively. t and t_0 are the flow times of polymer solution and of the pure solvent through the Ubbelohde viscometer. The intrinsic viscosities under theta conditions were estimated based on Qian et al. method [38].

3.4. Determination of nonsolvent/polymer interaction parameter

Nonsolvent/polymer interaction parameter, χ_{13}, was determined by equilibrium swelling measurement. PES films were prepared of about 0.2 g polymer flakes by a hot press at 250 °C. The films were then immersed in Petri dishes containing double-distilled water at 25 °C for one week. At certain time intervals, the polymer films were removed from water, dried between two filter papers, and weighed. This procedure was continued until no appreciable differences observed between two successive weight readings. Nonsolvent/polymer interaction parameter was then calculated from Eq. (21).

3.5. Membrane preparation

Homogeneous polymer solutions of 5, 12, and 20 wt% of PES in DMAc and NMP were cast on glass plates with uniform thickness by a doctor blade. Immediately after casting, the glass plates were immersed in a coagulation bath containing distilled water at 25 °C. After coagulation was completed, the solidified flat-sheet membranes were transferred to a second bath containing fresh water and then they were dried by placing them between sheets of filter paper.

3.6. SEM analysis

The cross section morphology of the prepared membranes was examined with a scanning electron microscope (Philips XL 30). The samples were fractured in liquid nitrogen, coated with gold in a sputtering device (SCD 005, BAL-TEC), and then transferred into the microscope chamber.

4. Results and discussion

4.1. Nonsolvent/solvent interaction parameters

The nonsolvent/solvent interaction parameters, g_{12}, have been considered concentration dependent.

For water/DMAc system, there are two completely different sets of g_{12} values in the literature. Shuguang et al. [40] and Gaides and McHugh [41] have used the vapor–liquid equilibrium data of Carli et al. [42] and reported two polynomial relations with different orders for g_{12} of water/DMAc system. On the other hand, Pesek and Koros [43] have used another source of vapor–liquid equilibrium data [44] and reported a different set of g_{12} values for this system. The latter authors have presented their results as a graph of g_{12} versus volume fraction of water, ϕ_1, but no relation has been presented for g_{12} in their paper. For water/NMP system, the most reliable data for g_{12} are those of Zeman and Tkacik [9]. We applied the data of Pesek and Koros (for water/DMAc) and Zeman and Tkacik (for water/NMP) to two polynomial relations and obtained the relation constants by least square method. For comparison, all the available g_{12} values and relations along with g_{12} relations derived in this study have been presented in Table 1 and Fig. 1.

Table 1
Concentration-dependent nonsolvent/solvent interaction parameter, g_{12}, of water/DMAc and water/NMP systems at 25 °C

System	g_{12}
Water/DMAc	$0.185 + 0.155u_2 - 1.02u_2^2 + 1.79u_2^3 - 1.10u_2^4$ [a]
	$0.164 + 1.54u_2 - 16.50u_2^2 + 90.24u_2^3 - 283.75u_2^4 + 530.74u_2^5 - 583.36u_2^6 + 347.72u_2^7 - 86.75u_2^8$ [b]
	0.58–0.9 [c]
	$0.8923 - 0.5911u_2 + 0.2821u_2^2$ [d]
Water/NMP	0.785–1.253 [e]
	$0.785 + 0.665u_2$ [f]
	$0.4860 + 0.8029u_2$ [g]

[a] Ref. [40].
[b] Ref. [41].
[c] Ref. [43].
[d] This study (based on data of Ref. [43]).
[e] Ref. [9] (for $x_2 = 0.1$–0.8, x_2 = mole fraction of NMP).
[f] Ref. [10] (based on data of Ref. [9]).
[g] This study (based on data of Ref. [9]).

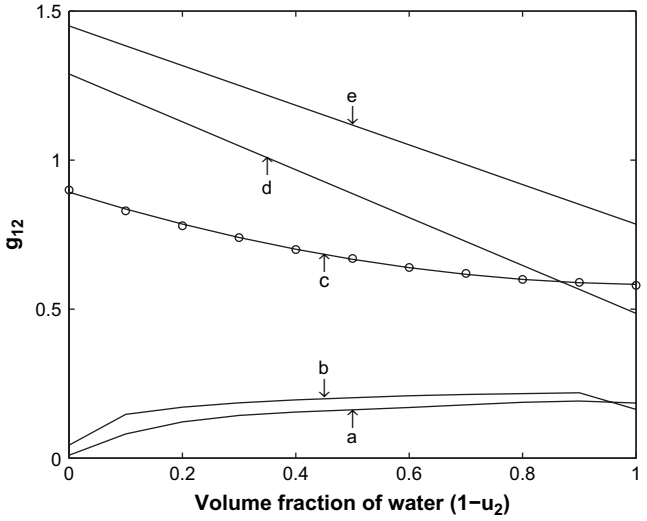

Fig. 1. Concentration-dependent interaction parameter of water/DMAc and water/NMP systems. (a) water/DMAc, Ref. [40]; (b) water/DMAc, Ref. [41]; (○) water/DMAc, Ref. [43]; (c) water/DMAc, this study based on the data of Ref. [43]; (d) water/NMP, this study based on the data of Ref. [9]; (e) water/NMP, Ref. [10].

Fig. 1 clearly shows that for water/DMAc system no appreciable differences are observed between data of Shuguang et al. and Gaides and McHugh but there is a significant difference between g_{12} values reported by these authors and data of Pesek and Koros. In our opinion, these differences might have been aroused from different sources of vapor–liquid equilibrium data that these authors used in their calculations. On the other hand, according to the results of Shuguang et al. and Gaides and McHugh, the g_{12} of water/DMAc system increases with the increase of water content which is opposite to the behavior of all other water–solvent systems reported in the literature (e.g. see Fig. 2 of Ref. [6]).

Although we have obtained different reports concerning g_{12} of water/DMAc system in the literature, Fig. 1 clearly shows that both the reported g_{12} values of the water/DMAc system are smaller than those of water/NMP system, which indicate that there is a better miscibility between water and DMAc compared to water and NMP system.

4.2. Solvent/polymer interaction parameters

The solvent/polymer interaction parameters, χ_{23}, were determined by the measurement of intrinsic viscosity according to Rudin model. In this method, the input parameters are intrinsic viscosity of the polymer in the desired solvent, its intrinsic viscosity under theta conditions, and polymer molecular weight. The results of Ubbelohde viscosity measurements for DMAc/PES and NMP/PES solutions are shown in Fig. 2. The intrinsic viscosity of these solutions can be determined by usual extrapolation of the results to zero concentration and the Huggins and Kraemer constants (k_H, k_K) can be determined from the slope of the corresponding straight lines. The results are shown in Table 2.

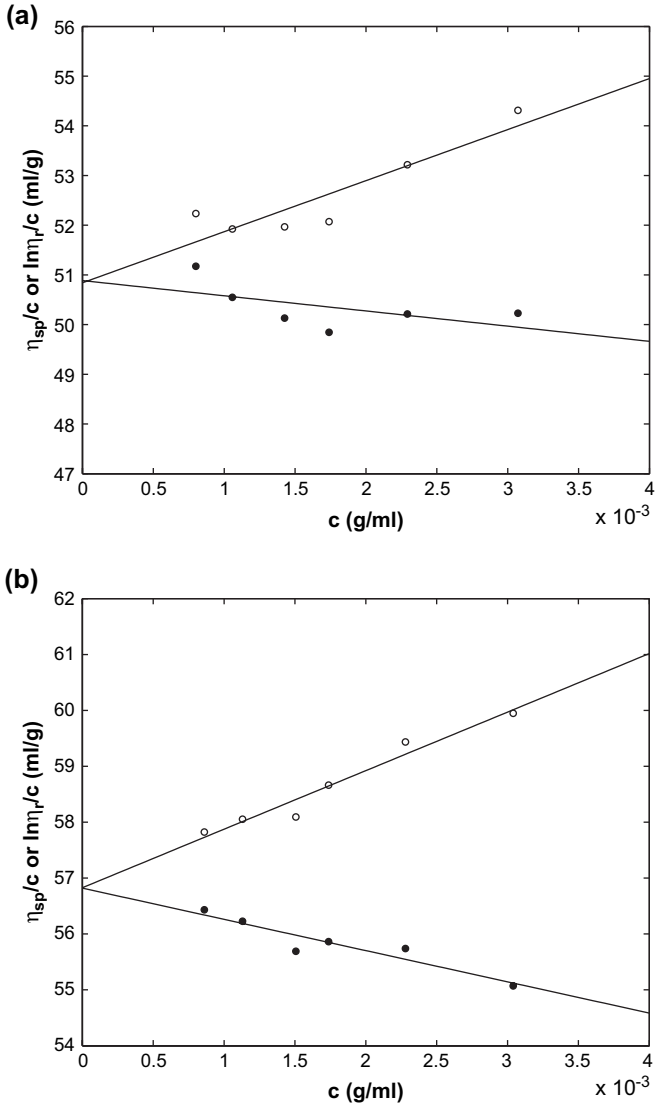

Fig. 2. Plot of η_{sp}/c (○) and $\ln\eta_r/c$ (●) versus c for (a) PES in DMAc and (b) PES in NMP at 25 °C.

k_H has values, which fall in the range of 0.3 (for good solvent–polymer pairs) to 0.5 (for poor solvent–polymer pairs). Meanwhile, the values of k_H and $k_H - k_K$ decrease and the intrinsic viscosity increases as solvent power increases [45]. The results of Table 2 show that k_H and $k_H - k_K$ values of DMAc/PES solution are slightly greater than those of NMP/PES solution. Furthermore, the intrinsic viscosity of DMAc/PES solution is lower than that of NMP/PES solution. Although both DMAc and NMP have been reported as good solvents for PES, our viscosity measurement results indicate that NMP is a better solvent for PES compared to DMAc.

Fig. 3 shows the results of intrinsic viscosity under theta conditions for PES/DMAc and PES/NMP solutions. The $[\eta]_\theta$ has been calculated with Qian et al. method [38]. This figure shows that $[\eta]_\theta$ is almost concentration independent and its average value is slightly lower for DMAc/PES solution compared to NMP/PES solution. For a better comparison, the average values of $[\eta]_\theta$ of these solutions have been presented in Table 2. Although it was observed that $[\eta]_\theta$ is concentration

Table 2
Results of viscometry measurements for DMAc/PES and NMP/PES solutions at 25 °C

Polymer solution	$[\eta]$ (ml/g)	k_H	k_K	$k_H - k_K$	$[\eta]_\theta$ (ml/g)
PES in DMAc	50.8663	0.3972	−0.1181	0.5153	25.8660
PES in NMP	56.8237	0.3244	−0.1731	0.4975	28.1493

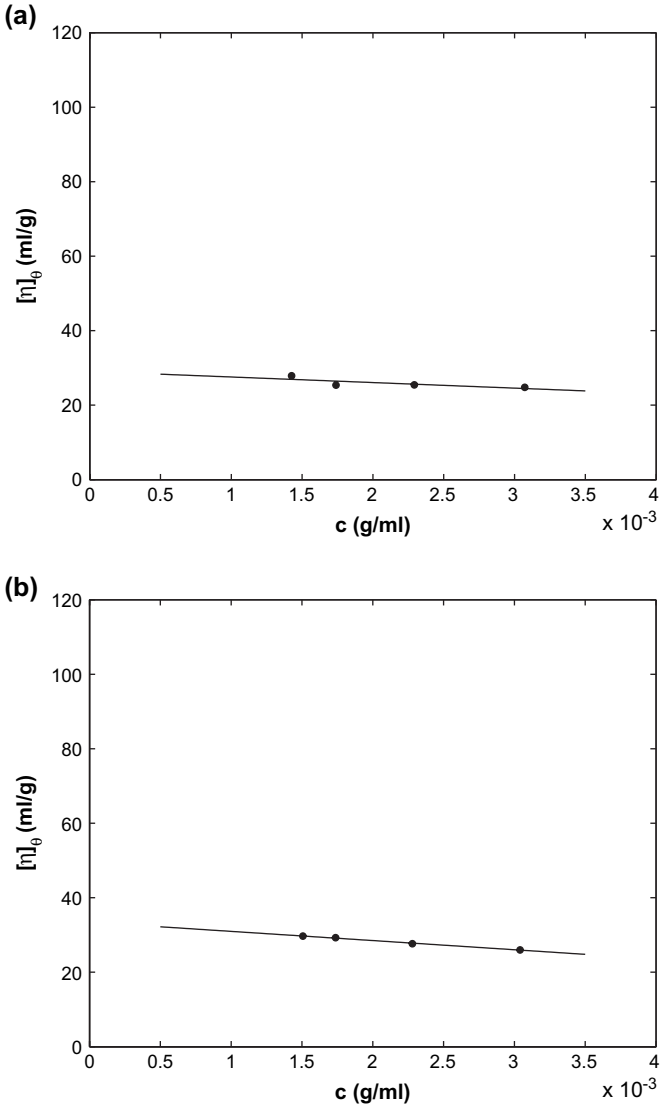

Fig. 3. Plot of $[\eta]_\theta$ versus c for (a) PES in DMAc and (b) PES in NMP at 25 °C.

independent, some deviations from straight line were observed for dilute region for both solutions. Such observations have been reported by Qian et al. [38] as well.

Now, second virial coefficients can be calculated from the above input parameters ($[\eta]$ and $[\eta]_\theta$) according to Rudin model, which in turn can be used for the estimation of χ_{23}. The results of χ_{23} calculation based on this method along with some data from the literature are presented in Table 3. The values of χ_{23} show that NMP/PES pair is more compatible than DMAc/PES pair. These results are in good agreement with our viscometry results.

Table 3
Solvent/polymer interaction parameter of DMAc/PES and NMP/PES solutions at 25 °C

Solution	χ_{23}
DMAc/PES	0.39[a]
NMP/PES	0.37[b]
DMAc/PES	–[c]
NMP/PES	0.36–0.55[d]

[a] This study.
[b] This study.
[c] No data was found.
[d] Ref. [9].

4.3. Nonsolvent/polymer interaction parameter

The nonsolvent/polymer interaction parameter, χ_{13}, has been determined by swelling method. For water/PES system we obtained a value of 2.83 for χ_{13} compared to the published values of 2.73 [9], 2.66 [46], and 2.70 [47]. To obtain χ_{13} values applicable to lower polymer concentrations, Zeman and Tkacik [9] used light scattering and refractive index measurements and found a value of 1.6 for χ_{13} of water/PES system.

4.4. Phase diagram of water/DMAc/PES and water/NMP/PES systems

Fig. 4 shows the experimental cloud point data for water/DMAc/PES and water/NMP/PES systems. As this figure shows, the cloud point curve of water/DMAc/PES system is closer to the polymer–solvent axis, and so less water is needed for the precipitation of PES in this system compared to water/NMP/PES system.

The observed results are totally reasonable because data of Tables 2 and 3 show that NMP is a better solvent for PES compared to DMAc and therefore a larger demixing gap should be observed for water/DMAc/PES system compared to water/NMP/PES system. On the other hand, as Fig. 1 shows,

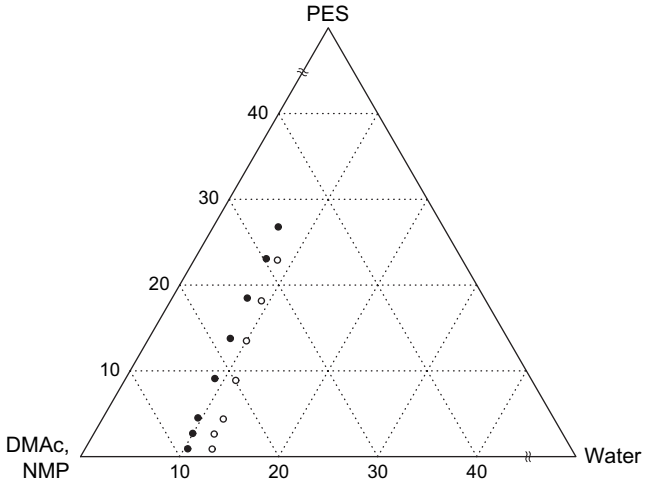

Fig. 4. Experimental cloud point data for water/DMAc/PES (●) and water/NMP/PES (○) systems at 25 °C.

g_{12} of water/NMP is higher than g_{12} of water/DMAc (better miscibility between DMAc and water) which again causes a broader homogeneous area for water/NMP/PES system. Therefore, the experimentally determined cloud point data of Fig. 4 are in accordance with the predicted interaction parameters of these systems. Similar cloud point results have been reported for these systems in the literature [9,48].

In Fig. 5 the theoretical binodal and spinodal curves along with experimental cloud point data for water/NMP/PES (Fig. 5a) and water/DMAc/PES (Fig. 5b) systems have been illustrated. The theoretical binodal and spinodal curves were constructed with numerical calculations based on an extended form of Flory–Huggins theory and the determined binary interaction parameter data.

First, we tried to construct a theoretical binodal curve with good agreement with experimental cloud point data for water/NMP/PES system. For χ_{13} and χ_{23} we used our experimentally determined data reported in the previous sections ($\chi_{13} = 2.83$ and $\chi_{23} = 0.37$). For g_{12} we used the concentration-dependent polynomial relation derived from data of Zeman and Tkacik [9] (Table 1).

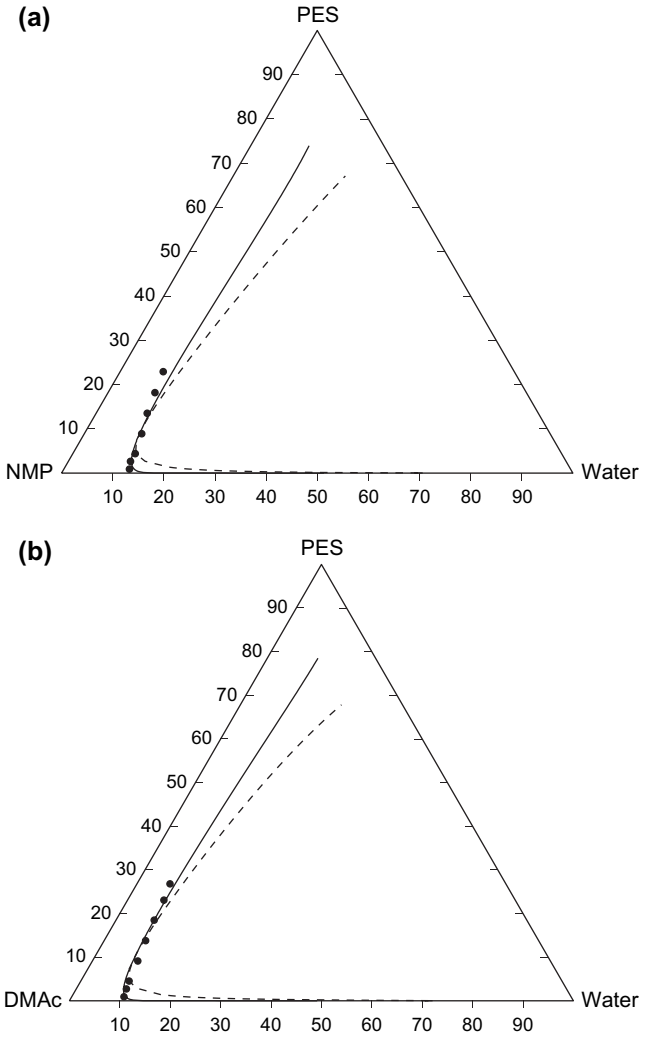

Fig. 5. Theoretical binodal (—) and spinodal (– – –) curves along with experimental cloud point data (●) for (a) water/NMP/PES ($g_{12} = 0.4860 + 0.8029u_2$, $\chi_{23} = 0.37$, $\chi_{13} = 1.6$) and (b) water/DMAc/PES ($g_{12} = 0.8923 - 0.5911u_2 + 0.2821u_2^2$, $\chi_{23} = 0.39$, $\chi_{13} = 1.6$) systems.

With these interaction parameter values we did not succeed to fit the theoretically constructed binodal curve with the experimentally determined cloud point data of this system. Therefore, we decided to change the interaction parameter values and find the best fit between binodal curve and cloud point data. We chose to alter the χ_{13} value, because in our opinion there is the largest uncertainty in determining this interaction parameter compared to other interaction parameters. We altered the χ_{13} value and found the best fit between the theoretical binodal curve and experimental cloud point data for $\chi_{13} = 1.6$. The resulting binodal and spinodal curves along with cloud point data of this system are illustrated in Fig. 5a. This value of χ_{13} for water/PES system is in a very good agreement with the data reported by Zeman and Tkacik [9] which has been measured with light scattering and refractive index measurements. According to the theoretical calculations performed by these authors they have found a χ_{13} of 1.5 for water/PES system.

Therefore, as the above results show, the equilibrium swelling measurement, which is usually used for the determination of nonsolvent/polymer interaction parameter (χ_{13}) of membrane-forming systems, does not seem a suitable method for determination of this parameter. Similar result has been reported for water/polysolfone (PSf) system as well [10].

We also evaluated the effect of changing the solvent/polymer interaction parameter (χ_{23}) value of this system on the binodal curve position, but it was observed that changing the χ_{23} value has minor effect in altering the position of binodal curve in the ternary phase diagram of water/NMP/PES system.

For water/DMAc/PES system we used χ_{13} value obtained from theoretical calculations performed for water/NMP/PES system. For g_{12} and χ_{23}, we used the values presented in Tables 1 and 3. As it has been mentioned in the previous sections, for water/DMAc system, there are two completely different sets of g_{12} values in the literature (Table 1). We examined both sets of the proposed g_{12} values with our numerical code and compared them with the experimental cloud point data of this system. The first set of g_{12} values [40,41], which have been presented as polynomial relations with different orders, were obtained from vapor–liquid equilibrium data of Carli et al. [42]. The second set of g_{12} values have been presented by Pesek and Koros [43]. The latter authors have presented their data as a graph of g_{12} versus volume fraction of water, ϕ_1, but no relation for g_{12} has been presented in their work.

First, the g_{12} relations proposed by Shuguang et al. [40] and Gaides and McHugh [41] were examined. With these relations and $\chi_{13} = 1.6$ and $\chi_{23} = 0.39$ we failed to fit the theoretical binodal curve with the experimental cloud point data. But, when we used the g_{12} relation derived from the data of Pesek and Koros [43] (Table 1), a very good agreement was found between theoretical binodal curve and cloud point data for this system (Fig. 5b). Therefore, according to our theoretical calculations, g_{12} values reported by Pesek and Koros [43] appear to be more reliable data for water/DMAc compared to those reported by Shuguang et al. [40] and Gaides and McHugh [41].

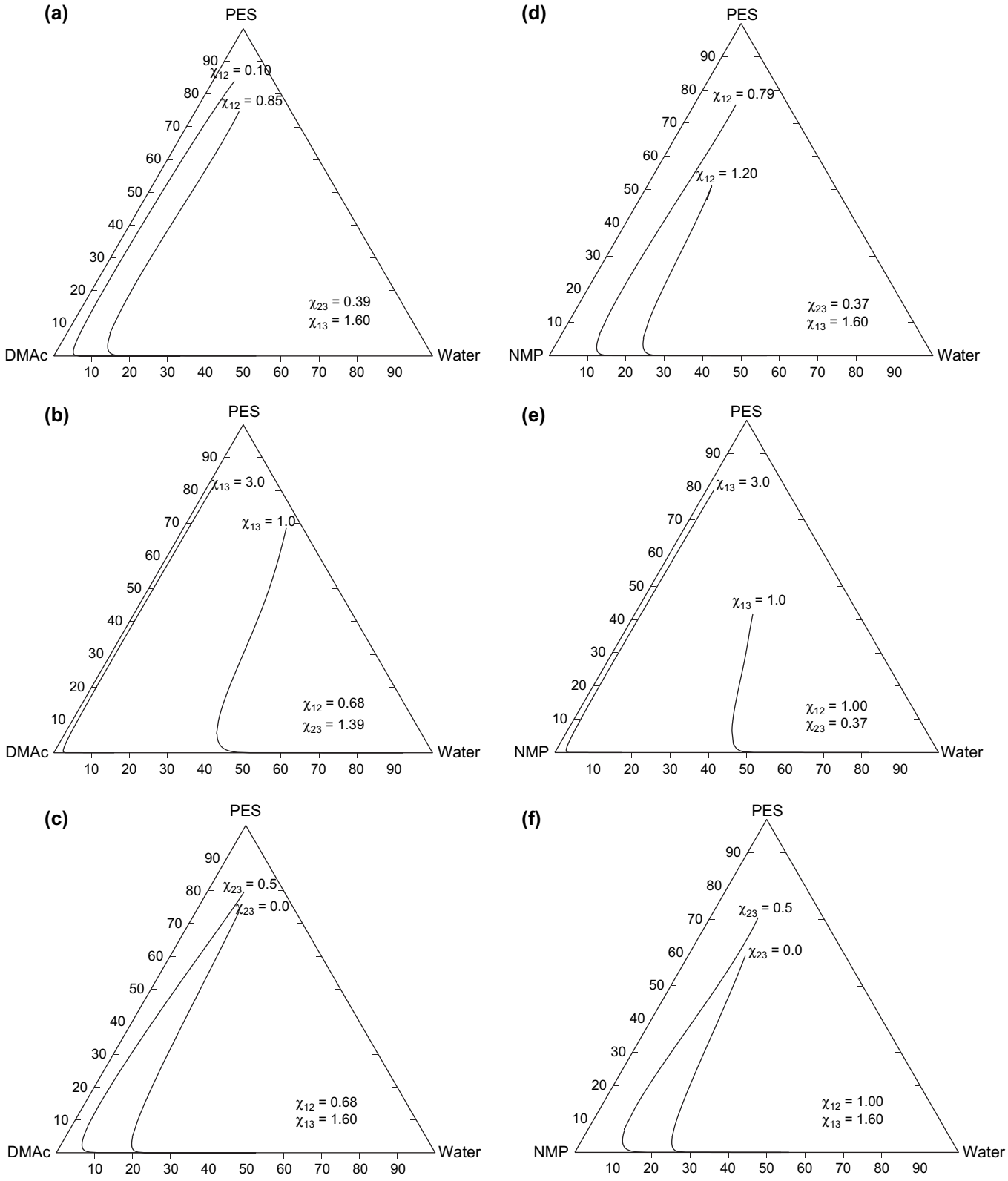

Fig. 6. Effect of variation of interaction parameters on the binodal curve positions for water/DMAc/PES (a, b, and c) and water/NMP/PES (d, e, and f) systems.

According to the determined interaction parameter values of water/NMP/PES and water/DMAc/PES systems, the critical point compositions of these systems calculated to be '10.68, 77.63, 11.69' and '7.88, 79.58, 12.54', respectively.

In Fig. 6, the effect of binary interaction parameter magnitudes on the binodal curve position is illustrated. Fig. 6 clearly shows that higher values of g_{12} (less compatibility between nonsolvent and solvent) and lower values of χ_{23} (better

compatibility between solvent and polymer) and χ_{13} (better compatibility between nonsolvent and polymer) shift the binodal curve toward the nonsolvent–polymer axis and produce larger homogeneous regions in the phase diagram of both systems. A detailed study concerning the effect of variation of interaction parameter magnitudes on the binodal and spinodal curve positions can be found in papers mainly devoted to this topic [6,8,10,11].

4.5. Membrane morphology

Morphology of the membranes prepared from ternary systems of water/DMAc/PES and water/NMP/PES is depicted in Fig. 7.

First, a comparison is made between morphology of the membranes prepared of these systems with varying concentrations of the polymer in the casting solution. Fig. 7 shows that the pores in the membranes prepared of solutions with low polymer concentration (5 wt%) have nearly channel-like structures with open ends for both systems (Fig. 7a,d). According to the critical point compositions calculated in the previous section, membranes prepared from polymer concentration of 5 wt% can be considered as good examples of membrane formation by spinodal decomposition [47]. Examination of these membranes revealed that these membranes lack the desired mechanical strength. Barth et al. [47] have pointed out that PES membranes prepared with low polymer concentrations (below 10 wt%) are not suitable membranes regarding

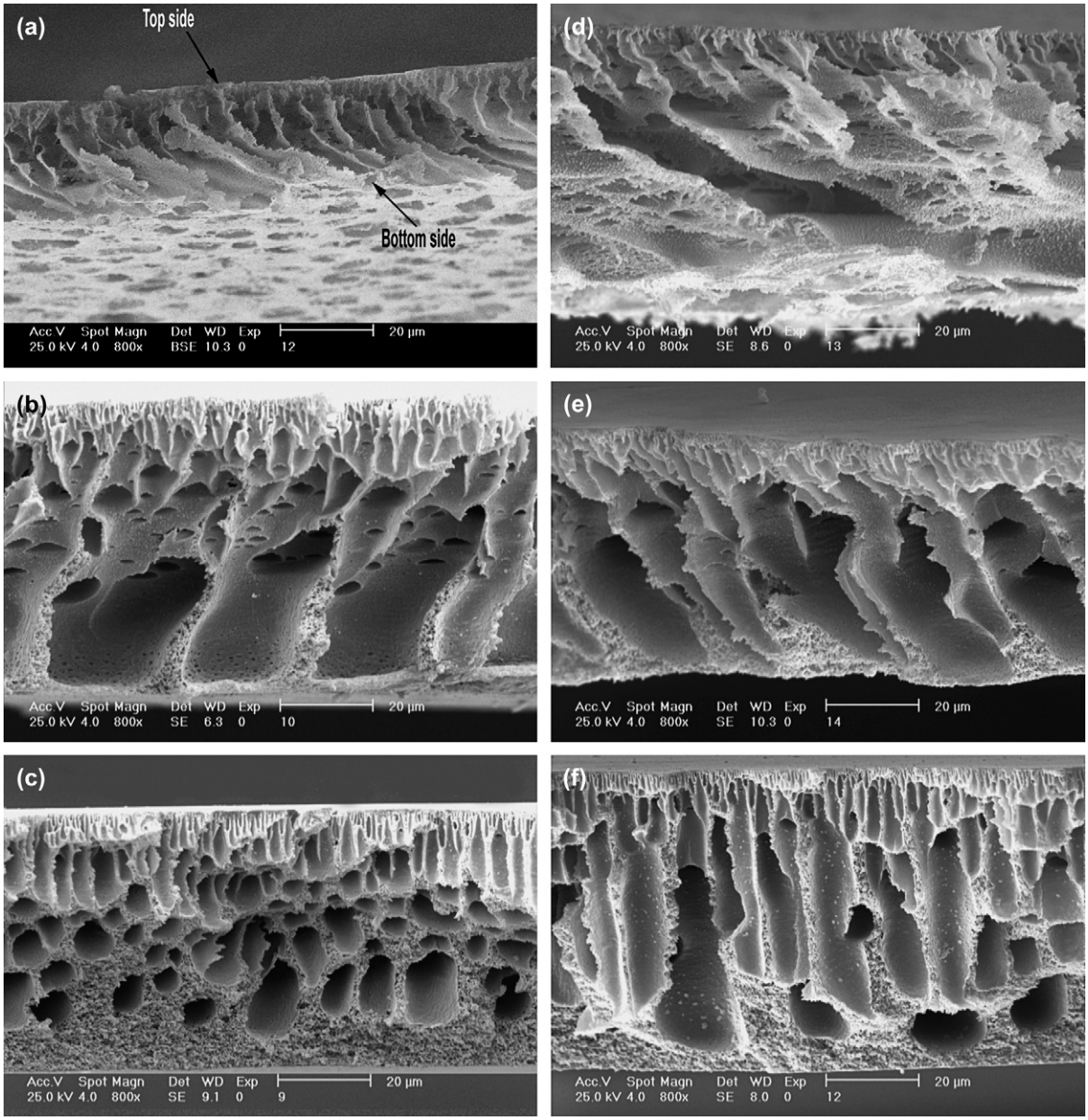

Fig. 7. SEM micrographs of the cross sections of different membranes prepared of the water/DMAc/PES and water/NMP/PES systems. Compositions of casting solutions were (a) 5 wt% PES in DMAc, (b) 12 wt% PES in DMAc, (c) 20 wt% PES in DMAc, (d) 5 wt% PES in NMP, (e) 12 wt% PES in NMP, and (f) 20 wt% PES in NMP.

mechanical strength and handling. When the polymer concentration increases, the membrane formation follows of nucleation and growth mechanism and the pores turn from large, open channels to medium size channels with closed ends (Fig. 7b and e) and small channel-, finger-, and tear-like structures (Fig. 7c and f). Therefore, increasing the polymer concentration leads to the creation of more sponge-like structures in the prepared membranes' morphology.

When the concentration of a polymer solution increases, its viscosity increases as well which causes a reduction in the nonsolvent/solvent exchange rate at the phase separation stage. There are several reports demonstrating that the changes in the nonsolvent/solvent exchange rate are the most important factors in determining the final structure of a membrane [20–22,49,50]. Increase of the exchange rate favors formation of the channel-like structures but decrease of the exchange rate favors formation of finger-, tear-, and sponge-like structures. Polymer concentration, viscosity of the casting solution, temperature of the polymer solution and the coagulation bath, and additives are the main factors, which alter the nonsolvent/solvent exchange rate [20,22,51].

Second, a comparison is made between structures of membranes prepared of two solvents of NMP and DMAc. As Fig. 7 shows membranes prepared of casting solutions with low polymer concentrations (5 wt%) have nearly the same channel-like structure for both the solvents used, but the size of channels in membranes prepared of DMAc is nearly smaller than those of NMP membranes. In concentration of 12 wt%, some of the channels turned to the finger-like structures but in membranes prepared of DMAc (Fig. 7b) the number of these finger-like structures are more than those of NMP membranes (Fig. 7e).

The difference between structures of membranes prepared of these two solvents can be better observed in the high polymer concentration of 20 wt% (Fig. 7c,f). A comparison between these two figures reveals that membrane prepared of DMAc as solvent has short fingers and tears with more sponge-like structures (Fig. 7c) but in membrane prepared of NMP (Fig. 7f) again some channels and fingers were observed.

It is widely accepted that high mutual affinity between nonsolvent and solvent and also other parameters which increase the nonsolvent–solvent exchange rate lead to the formation of more channel- and long finger-like structures [45,52]. In fact, Barton et al. have pointed out that strong nonsolvents lead to the formation of more finger-like structures, while nonsolvents with lower coagulation potential produce more homogeneous sponge-like structures [47,52]. As Fig. 1 shows, the nonsolvent/solvent interaction parameter (g_{12}) of water/NMP system is larger than g_{12} of water/DMAc system, and therefore interaction between water and DMAc is stronger than that of water and NMP. According to these statements, it was expected that the membranes prepared of DMAc as solvent must contain more channel-like structures compared to the membranes prepared of NMP, but SEM micrographs of Fig. 7 show the opposite results.

This unexpected observation can be explained as follows: PES is an amorphous polymer and it has been reported that for a ternary system containing an amorphous polymer,

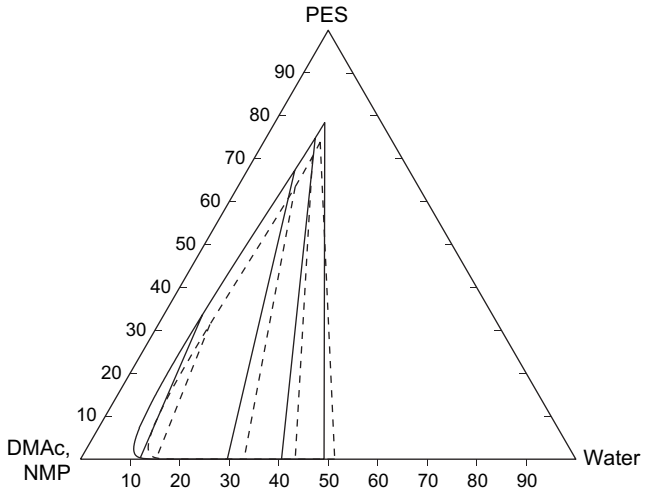

Fig. 8. Comparison of theoretical binodal and tie lines for water/DMAc/PES (—) and water/NMP/PES (– – –) systems.

vitrification of the polymer-rich phase is the only mechanism responsible for the structure fixation of membranes prepared by liquid–liquid demixing in an immersion precipitation process [23,53–55]. To compare the onset of the vitrification phenomena for these two systems, according to the theoretical calculations performed in the previous sections, the binodal curves and tie lines of these systems were calculated and represented in Fig. 8. As this figure shows, the tie lines of water/DMAc/PES system intersect the binodal curve of this system at a higher polymer concentration compared to those of water/NMP/PES system. It means that after liquid–liquid demixing, the polymer-rich phase of the water/DMAc/PES system vitrifies sooner than that of water/NMP/PES system and this phenomenon suppresses the growth of macrovoids in water/DMAc/PES system and a tear-like structure without any channels is formed for this system.

5. Conclusions

With the selection of appropriate binary interaction parameters, very good agreements were obtained between experimental cloud point data and theoretical binodal curves constructed based on Flory–Huggins theory for water/DMAc/PES and water/NMP/PES systems. Evaluation of nonsolvent/solvent interaction parameters showed that there is a much stronger interaction between water and DMAc compared to water and NMP. For water/DMAc system, there are two completely different sets of g_{12} values in the literature and our numerical calculations revealed that only one of these two sets can produce theoretical binodal curve that is in good agreement with experimental cloud point data for water/DMAc/PES system. Solvent/polymer interaction parameter determinations revealed that NMP is a better solvent for PES than DMAc. Meanwhile, our numerical calculations showed that equilibrium swelling measurement, which is typically used for determination of nonsolvent/polymer interaction parameter, is not a suitable method for the determination of this parameter.

SEM analysis of membranes prepared of these systems by phase separation technique showed that membranes prepared of NMP as solvent have typical channel-like structures but membranes prepared of DMAc have channel-like structures in low (5 wt%) and medium (12 wt%) polymer concentrations and tear-, finger- and sponge-like structures in high (20 wt%) polymer concentrations. Although affinity of DMAc/water pair is higher than NMP/water pair and it was expected that membranes prepared of the former system must contain more channel-like structures compared to the latter system, constructed theoretical binodal curve and tie lines of theses systems showed that this unexpected observation can be attributed to the early vitrification of the polymer-rich phase of DMAc system which suppresses the growth of macrovoids in this system.

Acknowledgements

The authors would like to acknowledge the financial support of Iran National Science Foundation (Grant no. 84122).

References

[1] Mulder M. Basic principles of membrane technology. Dordrecht: Kluwer Academic Publishers; 1991.
[2] Baker RW. Membrane technology and applications. England: John Wiley & Sons Ltd; 2004.
[3] Frommer MA, Feiner I, Kedem O, Bloch R. Desalination 1970;7:393–402.
[4] Frommer MA, Messalem RM. Ind Eng Chem Prod Res Dev 1973;12:328–33.
[5] Strathmann H, Koch K, Amar P, Baker RW. Desalination 1975;16:179–203.
[6] Altena FW, Smolders CA. Macromolecules 1982;15:1491–7.
[7] Wijmans JG, Kant J, Mulder MHV, Smolders CA. Polymer 1985;26:1539–45.
[8] Yilmaz L, McHugh AJ. J Appl Polym Sci 1986;31:997–1018.
[9] Zeman L, Tkacik G. J Membr Sci 1988;36:119–40.
[10] Kim JY, Lee HK, Baik KJ, Kim SC. J Appl Polym Sci 1997;65:2643–53.
[11] Lai J-Y, Lin S-F, Lin F-C, Wang D-M. J Polym Sci Polym Phys 1998;36:607–15.
[12] Flory PJ. Principles of polymer chemistry. Ithaca, NY: Cornell University Press; 1953.
[13] Tompa H. Polymer solutions. London: Butterworths; 1956.
[14] Sluma H-D, Passlack J, Buttner B, Scherf M. U.S. Patent 5,246,582; 1993.
[15] Bell C-M, Pirner M, Buck R, Gohl HJ. U.S. Patent 5,543,465; 1996.
[16] De Bartolo L, Morelli S, Lopez LG, Giorno L, Barbieri G, Salerno S, et al. Desalination 2006;199:147–9.
[17] Huang Z, Li Y, Wen R, Teoh MM, Kulprathipanja S. J Appl Polym Sci 2006;101:3800–5.
[18] Bonomini V, Berland Y. Dialysis membranes structure and predictions. Karger; 1995.
[19] Sakai K. J Membr Sci 1994;96:91–130.
[20] Barzin J, Madaeni SS, Mirzadeh H, Mehrabzadeh M. J Appl Polym Sci 2004;92:3804–13.
[21] Barzin J, Feng C, Khulbe KC, Matsuura T, Madaeni SS, Mirzadeh H. J Membr Sci 2004;237:77–85.
[22] Barzin J, Madaeni SS, Mirzadeh H. Iran Polym J 2005;14:353–60.
[23] Li S-G, van den Boomgaard Th, Smolders CA, Strathmann H. Macromolecules 1996;29:2053–9.
[24] Pouchly J, Zivny A, Solc K. J Polym Sci Part C 1968;23:245–56.
[25] Reuvers AJ, van den Berg JWA, Smolders CA. J Membr Sci 1987;34:45–65.
[26] Boom RM, van den Boomgaard Th, Smolders CA. J Membr Sci 1994;90:231–49.
[27] Prausnitz JM, Lichtenthaler RN, Gomes de Azevedo E. Molecular thermodynamics of fluid-phase equilibria. 2nd ed. Englewood Cliffs, NJ: Prentice-Hall; 1986.
[28] Kurata M. Thermodynamics of polymer solutions. Zuerich: Harwood Academic Publishers; 1982.
[29] Orwoll RA. Rubber Chem Technol 1977;50:451–79.
[30] Bonner DC. J Macromol Sci Rev Macromol Chem 1975;C13(2):263–319.
[31] Tseng HS, Lloyd DR. Polymer 1984;25:670–9.
[32] Durant YG, Sundberg DC, Guillot J. J Appl Polym Sci 1994;52:1823–32.
[33] Kok CM, Rudin A. J Appl Polym Sci 1981;26:3575–82.
[34] Kok CM, Rudin A. J Appl Polym Sci 1981;26:3583–97.
[35] Kok CM, Rudin A. J Appl Polym Sci 1982;27:353–62.
[36] Qian JW, Rudin A. Eur Polym J 1992;7:725–32.
[37] Billmeyer FW. Textbook of polymer science. New York: John Wiley & Sons, Inc; 1984.
[38] Qian JW, Wang M, Han DL, Cheng RS. Eur Polym J 2001;37:1403–7.
[39] Mulder MHV, Smolders CA. J Membr Sci 1984;17:289–307.
[40] Shuguang L, Chengzhang J, Yuanqi Z. Desalination 1987;62:79–88.
[41] Gaides GE, McHugh AJ. Polymer 1989;30:2118–23.
[42] Carli A, Di Cave S, Sebastiani E. Chem Eng Sci 1972;27:993–1001.
[43] Pesek SC, Koros WJ. J Membr Sci 1993;81:71–88.
[44] Gmehling J, Onken U. Vapor–liquid equilibrium data collection. Federal Republic of Germany: Dechema; 1986.
[45] Kim JH, Min BR, Won J, Park HC, Kang YS. J Membr Sci 2001;187:47–55.
[46] Singh VB, Barrie JA, Walsh DJ. J Appl Polym Sci 1986;31:295–9.
[47] Barth C, Goncalves MC, Pires ATN, Roeder J, Wolf BA. J Membr Sci 2000;169:287–99.
[48] Lau WWY, Guiver MD, Matsuura T. J Membr Sci 1991;59:219–27.
[49] Tam CM, Dal-Cin M, Guiver MD. J Membr Sci 1993;78:123–34.
[50] Dal-Cin MM, Tam CM, Guiver MD, Tweddle TA. J Appl Polym Sci 1994;54:783–92.
[51] Stropnik C, Musil V, Brumen M. Polymer 2000;41:9227–37.
[52] Barton BF, Reeve JL, McHugh AJ. J Polym Sci B Polym Phys 1997;35:569–85.
[53] Lin K-Y, Wang D-M, Lai J-Y. Macromolecules 2002;35:6697–706.
[54] Arnauts J, Berghmans H. Polym Commun 1987;28:66–8.
[55] Frank FC, Keller A. Polym Commun 1988;29:186–9.